ANL/CP--76649

DE92 019040

Thermodynamic Analysis of Phase Equilibria in the Iron–Zirconium System*

A. D. Pelton

Ecole Polytechnique, Montréal, Québec, Canada

L. Leibowitz and R. A. Blomquist

Argonne National Laboratory, Chemical Technology Division, 9700 S. Cass Avenue, Argonne, IL 60439 USA

Abstract: Continuing interest in development of metallic fuels for nuclear reactors has prompted an examination of the phase relations of many of the relevant binary and ternary systems of interest. We performed a thermodynamic analysis and optimization of the Fe–Zr system. Overall reasonably good agreement was found with published diagrams, but some significant changes were required to ensure thermodynamic consistency.

*This work supported by the U. S. Department of Energy

Thermodynamic Analysis of Phase Equilibria in the Iron–Zirconium System*

A. D. Pelton

Ecole Polytechnique, Montréal, Québec, Canada

L. Leibowitz and R. A. Blomquist

Argonne National Laboratory, Chemical Technology Division, 9700 S. Cass Avenue, Argonne IL 60439 USA

1. Introduction

An advanced reactor that employs a U–Pu–Zr alloy fuel is being developed. The potential advantages of this reactor are (1) a high degree of passive safety, resulting from use of the metallic fuel with a sodium coolant and (2) competitive economics, resulting from low costs for reactor construction and fuel recycle Because the alloy fuel will be clad in stainless steel, there is particular interest in phase diagrams of fuel and stainless steel components, particularly iron. In previous work, we presented our assessments of the U–Zr [1], Fe–U [2], and Pu–U [3] phase diagrams and this effort is continued here with our assessment of the Fe–Zr system.

Massalski [4] presented the Fe–Zr diagram shown in Fig. 1, which was derived by Arias and Abriata [5]. Kubaschewski [6] gave a somewhat different Fe–Zr diagram shown in Fig. 2. We undertook a thermodynamic study of this system because of its complexity and the apparent uncertainties in some of the phase relations

2. Calculational Method

The general methods used in our analysis have been discussed previously [1–3] and will only be summarized here. The calculations are performed with programs of the F*A*C*T (Facility for the Analysis of Chemical Thermodynamics) computer system based in Montreal [7,8] and involve determining equations for the Gibbs energy of all phases existing in a system as functions of temperature and composition. A least squares optimization of all

*This work supported by the U. S. Department of Energy

available thermodynamic data provides a self-consistent polynomial power series for the thermodynamic properties. Binary phase diagrams are derived from the thermodynamic properties of the phases by calculating the lowest common tangents to the Gibbs energy-composition curves. This procedure ensures thermodynamic consistency of the resulting phase diagram and provides a powerful means for assessing conflicting data.

3. Thermodynamic Calculations

3.1. Free Energies of Pure Zr and Fe

The Gibbs energies of transition for pure Fe and Zr were required in this analysis. The equations for the Gibbs energy of transition ΔG°(transition), of iron were taken from the JANAF tables [9] and are the same as used previously in our analysis of the Fe-U system [2]. As before we have neglected magnetic transitions. Iron has three allotropes: α, δ, and γ. The α and δ forms have a body-centered cubic (bcc) structure while the γ form is face-centered cubic (fcc). The equations for Gibbs energies of transition are given below, where the subscript ℓ represents liquid:

$$\Delta G^\circ(\mathrm{Fe}, \alpha \rightarrow \gamma) = 900. - 0.761T \tag{1}$$

$$\Delta G^\circ(\mathrm{Fe}, \gamma \rightarrow \delta) = 836.8 - 0.502T \tag{2}$$

$$\Delta G^\circ(\mathrm{Fe}, \delta \rightarrow \ell) = 13807 - 7.632T \tag{3}$$

Here ΔG°(transition), is in joules/mole, and T is in Kelvin.

The equations for the Gibbs energies of transition of zirconium used in the present work are the same as those used earlier [1] and were taken from the compilation of Hultgren [10]. There are two allotropes of solid zirconium: hexagonal Zr(α) and bcc Zr(β). The equations for Gibbs energies of transition are

$$\Delta G^\circ(\mathrm{Zr}, \alpha \rightarrow \beta) = 7273.5 - 27.008T + 2.929T \ln T \tag{4}$$

$$\Delta G^\circ(\mathrm{Zr}, \beta \rightarrow \ell) = 9656.7 + 68.927T + 23.012 \times 10^{-4}T^2 - 10.234T \ln T \tag{5}$$

3.2. Properties of the liquid phase

In optimizing the properties of the liquid, we chose one point on the iron-liquidus curve, namely, the eutectic point at 8.8 at.% Zr and 1335°C from Fig. 2. The eutectic

given in Fig. 1, 9.8 at.% Zr and 1337°C, is within expected uncertainties. One point on the zirconium–liquidus curve was also chosen, namely the eutectic point from Fig. 1 (76 at.% Zr and 928°C) in equilibrium with solid Zr(β) with an activity (a^{β}_{Zr}) of 0.94. Figure 2 gives the eutectic at the same composition but 947°C. We have accepted the judgment of Abriata and Arias on this point. From these two eutectics the liquidus was optimized as a sub-regular solution with excess entropy (s^E) and excess enthalpy (h^E) given by:

$$s^E(\ell) = 0 \tag{6}$$

$$h^E(\ell) = X_{Fe}X_{Zr}(-66984 - 29050X_{Zr}) \tag{7}$$

where X indicates the atom fraction of the subscripted element.

Sudavtsova et al. [11] used solution calorimetry to measure h^E for Fe–rich solutions. At $X_{Zr} = 0.4$ they report $h^E \approx -23$ kJ/mol, whereas Equation 7 yields −19 kJ/mol, in reasonable agreement with the calorimetry. From mass spectrometry measurements Wagner and St. Pierre [12] determined h^E for the similar liquid Fe–Ti alloys and found $h^E = -40585X_{Fe}X_{Ti}$ J/mol and $s^E \approx 0$. Equations 6 and 7 are thus quite reasonable.

3.3. Solubility of Zr in Fe(δ)

Figure 1 shows 4.5 at.% solubility of Zr in Fe(δ) at 1357°C, while Fig. 2 shows less than 1 at.% solubility at 1355°C. By assuming negligible solubility of Zr in Fe(γ), we can calculate the transformation point depression using Eq. 2 and Raoult's Law. The depression was calculated as 39°C corresponding to a solubility of 0.15 at.%, in support of Fig. 2.

3.4. Solubility of Fe in Zr

Both Figs. 1 and 2 indicate negligible solubility of Fe in Zr(α). In the present analysis zero solubility was assumed. Figure 1 gives a transformation point depression to 730°C at 4.0 at.% Fe, while Fig. 2 shows a depression to 795°C at 3.55 at.% Fe . The former requires fairly large positive deviations from ideality in Zr(β), and the latter requires fairly large negative deviations In the present analysis, we assumed that Zr(β) is a Henrian solution (*i.e.*, the

activity of Zr was ideal). Kubaschewski's eutectoid temperature of 795°C [6] was retained. The calculated eutectoid composition is 97.3 at.% Zr, which is within the experimental error limits.

3.5. Fe(δ) and Zr(β) Henrian Solutions

If we calculate the Henrian activity coefficient of Zr in Fe(δ) to reproduce the catatectic temperature of 1355°C and the Henrian activity coefficient of Fe in Zr(β) to reproduce the solidus at 94 at.% Zr and 928°C then

$$RT \ln \gamma_{Zr}[Fe(\delta)] = -19514 + 8.0T \tag{8}$$

$$RT \ln \gamma_{Fe}[Zr(\beta)] = -42677 + 8.0T \tag{9}$$

These activity coefficients are with respect to pure liquid Zr and Fe as standard states. The entropic terms used in deriving Eqs. 8 and 9 were set equal to 8.0 J/(mol·K), because this value is close to the average entropy of fusion of most metals.

4. Phase Equilibria Calculated for Intermetallic Compounds

4.1. Fe_2Zr

As reported by Arias and Abriata [5], the enthalpy of formation of Fe_2Zr from the solid elements has been measured calorimetrically as −29.7 kJ/mol of atoms at 1487°C [13] and as −24.7 kJ/mol of atoms at 750°C [14]. Within the error limits of the measurements, the enthalpy of formation may be assumed to be independent of temperature. We take the more recent value [13] and change it to the liquid standard state with Eqs. 3 and 5. The calculated enthalpy of formation from the liquid elements is −46.4 kJ/mol of atoms. The melting point of 1675°C permits the Gibbs energy of formation at this temperature to be calculated. The result in joules per mole of atoms for the reaction $2/3Fe(\ell) + 1/3Zr(\ell) = 1/3Fe_2Zr(s)$ is:

$$\Delta G^\circ = -46442 + 9.8T \tag{10}$$

The magnitude of the entropy used in Eq. 10 is reasonable for an entropy of fusion. The non-stoichiometry of Fe_2Zr is shown in Fig. 2 as extending from 29 to 36 at.% Zr at temperatures

near 1450°C. In Fig. 1, the range of stoichiometry for Fe_2Zr is based upon the work of Svechnikov et al. [15] (27.7 to 34.3 at.% Zr at 1450°C). However, Aubertin et al. [16] measured nearly the same range of stoichiometry (27.1 to 34 at.% Zr) in samples quenched from 700°C. It is unlikely that the range of stoichiometry should remain so constant with temperature. Past experience and thermodynamics indicate that the range should narrow with decreasing temperature. Aubertin et al. [16] support a stoichiometry range from 27 to 34 at.the range of homogeneity at 1482°C is from 27.6 to 33.3 at.% Zr. That is, it is assumed that Zr is insoluble in Fe_2Zr.

The Fe_2Zr phase was modeled with a general defect model recently developed for non-stoichiometric phases [17]. The parameters of this model are the energies of formation of the majority point defects on either side of the stoichiometric composition. The exact nature of the defects need not be specified. If the energy of formation is very large, then the range of stoichiometry on that side of the stoichiometric composition is very narrow. The smaller the energy of formation of a defect, the wider the range of stoichiometry. The present optimization uses the following Gibbs energies of formation of defects on the Fe-rich and Zr-rich sides (ΔG_1 and ΔG_2 respectively, in J/mol):

$$\Delta G_1 = 147591 - 20.9T \tag{11}$$

$$\Delta G_2 = 251040 \tag{12}$$

This yields a range of stoichiometry from 27.6 to 33.3 at.% Zr at 1482°C, as shown in Fig. 3. (Effectively, ΔG_2 is extremely large.) A small temperature dependence was included in Eq. 11. Without this term the calculated range of stoichiometry widens to slightly below 25 at.% Zr near 1300°C, thereby swamping the Fe_3Zr phase before narrowing again at lower temperatures. (However, see discussion of the Fe_3Zr phase.)

The calculated liquidus composition at 1482°C is 14.1 at.% Zr, as shown in Fig. 3. This is in excellent agreement with the value of 13.7 at.% shown in Figs. 1 and 2. In this composition region, the liquidus is quite accurately known [5,6]. This good agreement

supports the optimization of the properties of the liquid and the Fe_2Zr phase as given in Eqs. 6, 7, and 10–12. On the Zr–side, the liquidus of Fe_2Zr is not well known. The liquidus shown in Fig. 1 [5] was taken from Ref. 15 and that in Fig. 2 [6] is based upon estimates by Rhines and Gould [18]. The calculated liquidus in Fig. 3 descends somewhat more steeply. At 1100°C, for example, the calculated liquidus composition is 62 at.% Zr, whereas in Fig. 2 this composition is 66.5 at.% Zr. Basically, the rate of decrease of the liquidus temperature with composition on either side of the stoichiometric Fe_2Zr composition is determined by the same enthalpy of formation given in Eq. 10. The liquidus cannot descend more steeply on one side than the other. Furthermore, the liquidus on the Fe–rich side is in excellent agreement with the calorimetrically measured enthalpy of formation, Eq. 9. The less steep liquidus of Figs. 1 and 2 could be reproduced by postulating a wide stoichiometry range of Fe_2Zr extending to about 40 at.% Zr at 1100°C. This, however, is contrary to reported measurements. By introduction of more enthalpic and/or entropic terms for the excess Gibbs energy of the liquid in Eqs. 6 and 7 it might also be possible to force a fit, but this is felt to be unjustified. Note that the calculated liquidus, Fig. 3, does not contradict any measured points. Because the liquidus in this region in Figs. 1 and 2 is based only upon estimates, we conclude that the calculated steeper liquidus in Fig. 3 is probably correct. This is an area in which more measurements would be useful.

4.2. $FeZr_2$ and $FeZr_3$

The $FeZr_3$ phase shown in Fig. 1 is based mainly on the work of Malakhova and co–workers [19,20] and by Aubertin et al. [16]. These authors do not report $FeZr_4$. However, several authors have reported both $FeZr_3$ and $FeZr_4$, and Kubaschewski [6] in Fig. 2 proposes tentatively that $FeZr_4$ rather than $FeZr_3$ is stable at high temperatures. Aubertin et al. [16] in a recent study observed only $FeZr_3$. In the present analysis only $FeZr_3$ was considered. The compound was assumed stoichiometric.

The stoichiometry of $FeZr_2$ was reported [19,20] to vary between 66.7 and 69 at.% Zr, as shown in Fig. 1. In the present analysis, this compound was assumed to be stoichiometric.

In Fig. 2, the compound is shown as always Fe–rich, narrowing to a stoichiometry near 62.5 at.% Zr at lower temperatures. No explanation for this behavior was given by Kubaschewski [6]. In any case, this is only stoichiometry indicated tentatively by dashed lines in Fig. 2.

The following Gibbs energies of formation of $FeZr_2$ and $FeZr_3$ (in J/mol of atoms) from the liquid elements were chosen: for $1/3Fe(\ell) + 2/3Zr(\ell) = 1/3FeZr_2(s)$ we have

$$\Delta G^\circ = -38158 + 9.6T \tag{13}$$

and for $1/4Fe(\ell) + 3/4Zr(\ell) = 1/4FeZr_3(s)$

$$\Delta G^\circ = -42007 + 16.7T \tag{14}$$

As shown in Fig. 3, the eutectic reported at 928°C [5], the eutectoid reported at 795°C [6], and the peritectoid reported at 885°C [5] are well reproduced. $FeZr_2$ is calculated to melt congruently at 998°C with a eutectic at 995°C and 64.4 at.% Zr. That is, the melting is just at the limit between being congruent and incongruent. The incongruent melting at 974°C shown in Fig. 1 is based upon DTA (cooling curve) studies by Malakhova and Kobylkin [19], who observed thermal arrests in the range 967°C to 987°C. Although they interpreted these arrests as being due to a peritectic reaction, they could equally well be interpreted as indicating a eutectic reaction. No arrests were observed at compositions richer in Zr than the $FeZr_2$ composition. This supports the present interpretation of a eutectic reaction. The temperature of 974°C shown in Fig. 1 [5] was taken as the average of the temperatures of the thermal arrests, which were observed over the range 967°C to 987°C. However, it would be more correct to take the highest observed temperature (987°C) as the true temperature, since undercooling can easily give spuriously low readings during cooling curve experiments, but spuriously high readings are harder to explain. Our calculated invariant temperature of 995°C agrees with the reported temperature within experimental error limits.

When converted to a standard state of Fe(γ) and Zr(β) via Eqs. 2–5, the enthalpy of formation of $FeZr_2$ from the solids at 1000°C is −20.7 kJ/mol of atoms, which is very close to

the value of −20 kJ/mol of atoms calculated by Colinet et al. [21]. In addition, the entropy of fusion of $FeZr_3$ in Eq. 13 is nearly identical to that of Fe_2Zr in Eq. 10. Hence, Eq. 13 seems reasonable. The entropy of fusion of $FeZr_3$ of 16.7 J/(mol·K) of atoms in Eq. 14, while rather large, is not unreasonable if $FeZr_3$ is an ordered compound.

A eutectoidal decomposition of $FeZr_2$ at 554°C was calculated. From X-ray and micrographic analysis, Malakhova and Kobylkin [19] report the eutectoid near 775°C, as shown in Fig. 1. Aubertin et al. [16] found no $FeZr_2$ phase when Fe and Zr were annealed together at 700°C for 24 hours, but they did observe the phase at 900°C.

From Eqs. 10, 13, and 14, we find that ΔG^o for the decomposition of $FeZr_2$ to Fe_2Zr and $FeZr_3$ is only about 800 J/g-atom at 700°C. Small changes in the Gibbs energies of the compounds cause large changes in the calculated eutectoid temperature. A set of Gibbs energies can easily be obtained from Eqs. 10, 13, and 14 which yields a eutectoid at 775°C. However, this can only be accomplished at the expense of changing another calculated invariant temperature (*e.g.*, the 928°C eutectic, the melting point of $FeZr_2$, or the 796°C eutectoid) by about 10°C. Accurately measuring a eutectoid decomposition temperature is very difficult because of the very slow kinetics and the small driving force. The measurement technique (anneal and observe), involving relatively short annealing times, tends to give errors suggesting too high a eutectoid temperature. More experimental work should be done, involving very long annealing times, to find the true eutectoid temperature.

4.3. Fe_3Zr

The Gibbs energy of formation of Fe_3Zr was chosen to give a peritectic temperature of 1482°C and a eutectic at 1335°C and 8.8 at.% Zr. For the reaction $3/4Fe(\ell) + 1/4Zr(\ell) = 1/4Fe_3Zr$,

$$\Delta G^\circ = -34636 + 6.422T \qquad (15)$$

in J/mol of atoms. The entropy term in Eq. 15 is reasonable for an entropy of fusion. As seen in Fig. 3, the calculations predict that Fe_3Zr decomposes eutectoidally below 1175°C. However, this results from small differences among the Gibbs energies of the solid phases.

Within the error limits of the optimization, a eutectoid temperature cannot be calculated with any precision.

Aubertin et al. [16] did not observe this compound when the elements were annealed at 950°C. They propose that the compound may only exist above 950°C. This would be consistent with the present calculations. Alternatively, they propose that Fe_3Zr is actually not a stable compound and may only result from contamination of the specimens. In this context, note that the reported eutectic temperature and composition can easily be fitted without Fe_3Zr. By changing Eq. 11 to $\Delta G_1 = 110876$ J/mol, which gives about the same ΔG_1 at 1482°C as in Eq. 11, a eutectic at 1339°C is calculated. Furthermore, in this case, one less parameter is required.

5. Discussion

All the available data on the Fe–Zr system are generally well correlated by our optimized phase diagram which is based on reasonable and simple thermodynamic expressions. The analysis predicts a liquidus in the range from 33.3 to 67 at.% Zr, which is lower than the estimated liquidus in the literature. If the calculated liquidus were higher, then the Gibbs energy of formation of $FeZr_2$ could be reduced somewhat. This would cause an increase in the calculated eutectoid temperature of 554°C. On the other hand, raising the liquidus temperature would require a more complex expression for s^E and/or h^E in Eqs. 6 and 7. Measurements of the liquidus temperature at one or two points in this composition region would be useful.

Acknowledgments

The authors wish to express there appreciation to Paul Talley (Ecole Polytechnique) for his computational and programming assistance.

References

1. L. Leibowitz, R. A. Blomquist, and A. D. Pelton, J. Nucl. Mater. 167 (1989) 76.
2. L. Leibowitz and R. A. Blomquist, J. Nucl. Mater. 184 (1991) 47.
3. L. Leibowitz, R. A. Blomquist, and A. D. Pelton, J. Nucl. Mater. 184 (1991) 59.
4. T. B. Massalski, Ed., Binary Alloy Phase Diagrams, 2 ed., American Society for Metals, Metals Park, OH (1990).
5. D. Arias and J. P. Abriata, Bull. Alloy Phase Diagrams 9 (1988) 597.
6. O. Kubaschewski, Iron–Binary Phase Diagrams, Springer–Verlag, New York, p. 175 (1982).
7. C. W. Bale, A. D. Pelton, and W. T. Thompson, F*A*C*T Guide to Operations, McGill University/Ecole Polytechnique, Montreal (1985).
8. A. D. Pelton, Physical Metallurgy, 3rd ed., R. W. Cahn and P. Haasen Eds., North–Holland, New York, p. 328 (1983).
9. M. W. Chase, Jr. , C. A. Davies, J. R. Downey, Jr. , D. J. Frurip, R. A. McDonald, and A. N. Syverud, JANAF Thermochemical Tables, 3rd ed., Nat'l Bureau of Standards, Washington (1986).
10. R. Hultgren, P. D. Desai, D. T. Hawkins, M. Gleiser, and K. K. Kelley, Selected Values of the Thermodynamic Properties of Binary Alloys, American Society for Metals, Menlo Park, OH (1973).
11. V. S. Sudavtsova, V. P. Kurach, and G. I. Batalin, Russ. Metall. No. 3 (1987) 60.
12. S. Wagner and G. R. St.Pierre, Met. Trans. 5 (1974) 887.
13. J.C. Gachon and J. Hertz, Calphad 7 (1983) 1.
14. A. Schneider, H. Klotz, J. Stendel, and G. Strauss, Pure Appl. Chem. 2 (1961) 13.
15. V. N. Svechnikov, V. M. Pan, and A. Ts. Spektor, Russ. J. Inorg. Chem. 8 (1963) 1106.
16. F. Aubertin, U. Gonser, S. J. Campbell, and H.-G. Wagner, Z. Metallkd. 76 (1985) 237.

17. L. Li and A. D. Pelton, to be published.

18. R. N. Rhines and R. W. Gould, Adv. X-Ray Anal. 6 (1963) 62.

19. T. O. Malakhova and Z. M. Alekseyeva, J. Less-Common Metals 81 (1981) 293.

20. T. O. Malakhova and A. N. Kobylkin, Russ. Metall. No. 2 (1982) 187.

21. C. Colinet, A. Pasturel and P. Hicter, Calphad 9 (1985) 71.

List of Figures

Fig. 1 Fe–Zr phase diagram as assessed by Arias and Abriata [5] Reproduced from Ref. 4, with permission.

Fig. 2 Fe–Zr phase diagram as assessed by Kubaschewski [6], Reproduced with permission.

Fig. 3 Optimized Fe–Zr phase diagram.

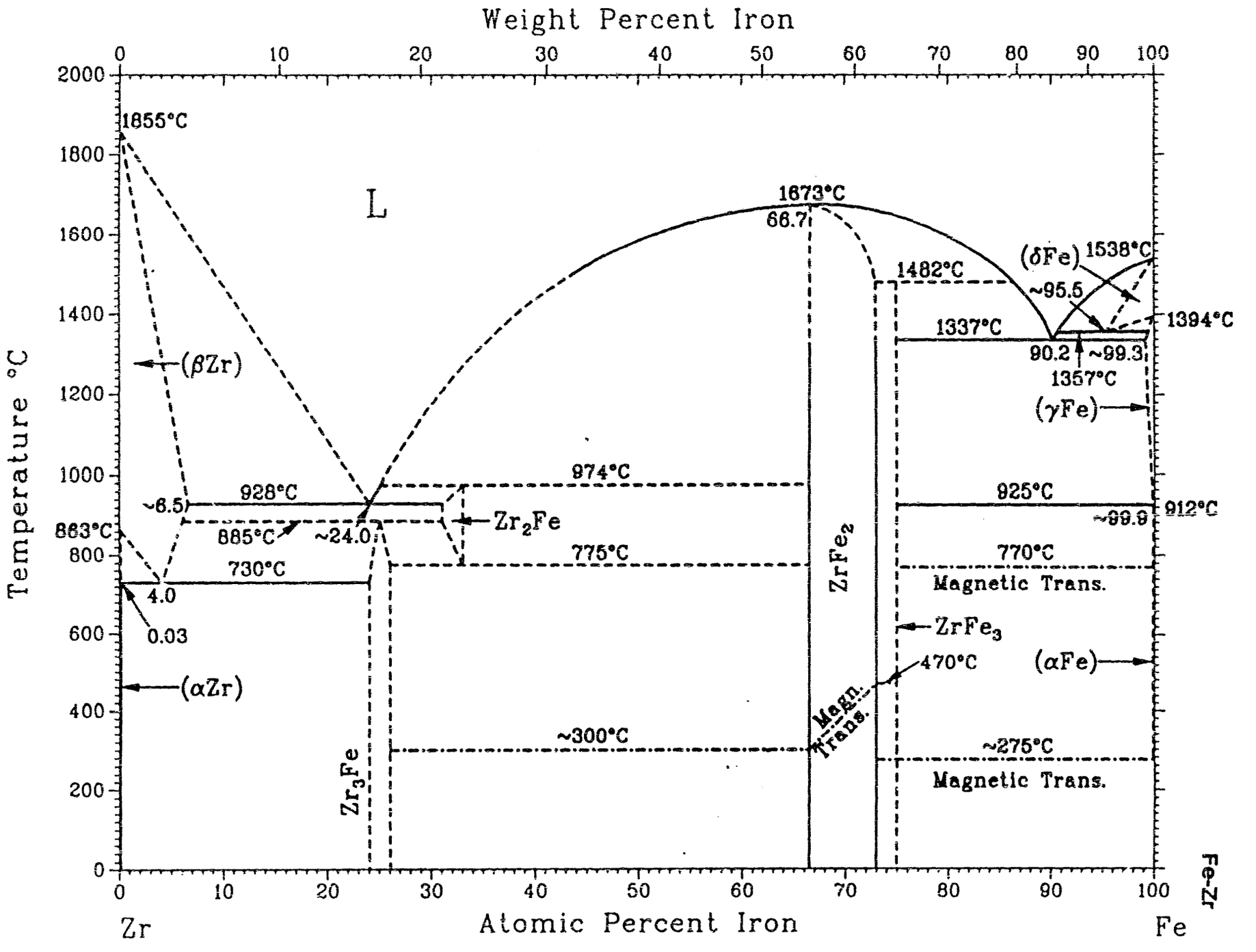

Fig. 1: Fe-Zr phase diagram as assessed by Arias and Abriata [88Ari].

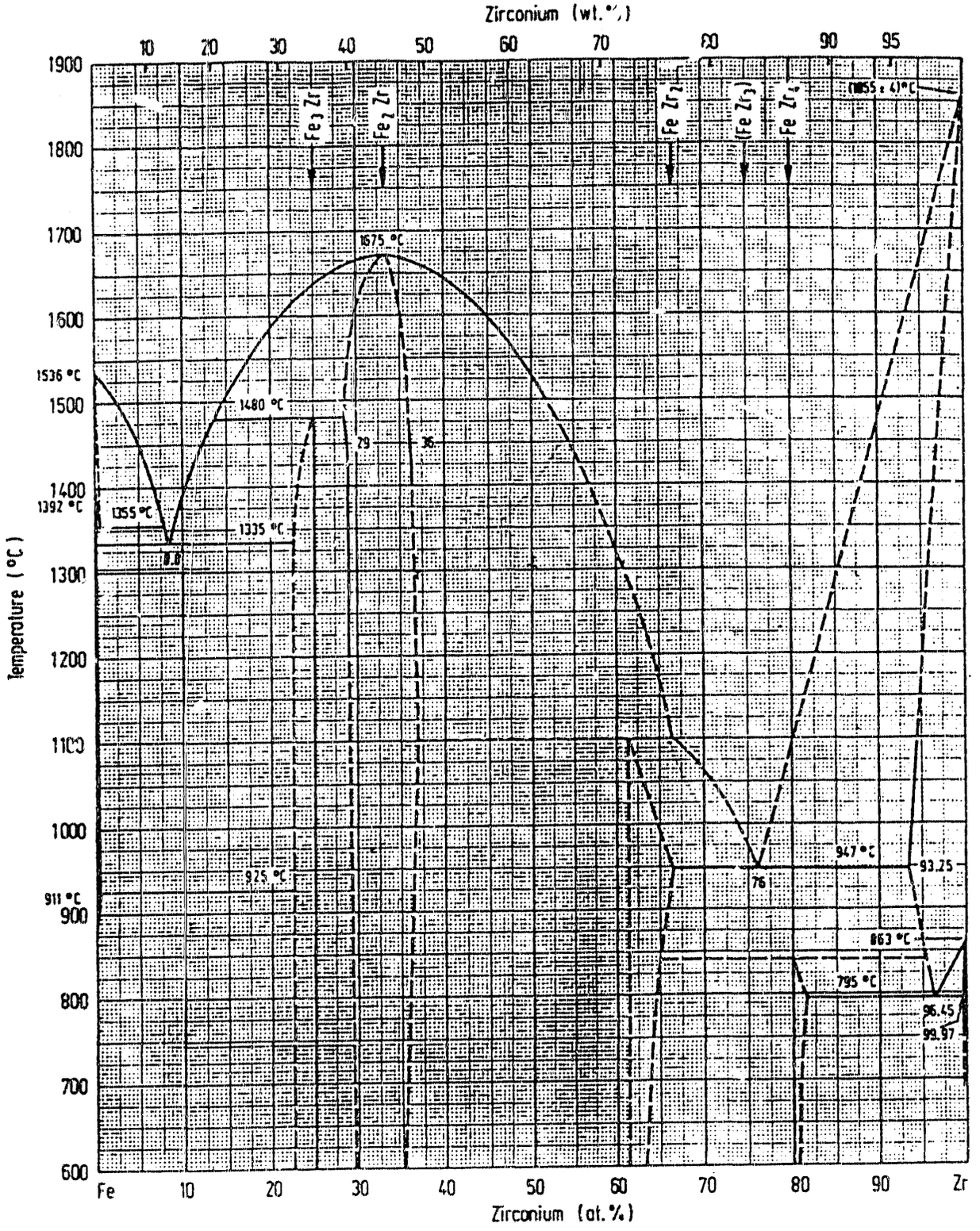

Fig. 2: Fe-Zr phase diagram as assessed by Kubaschewski [82Kub].

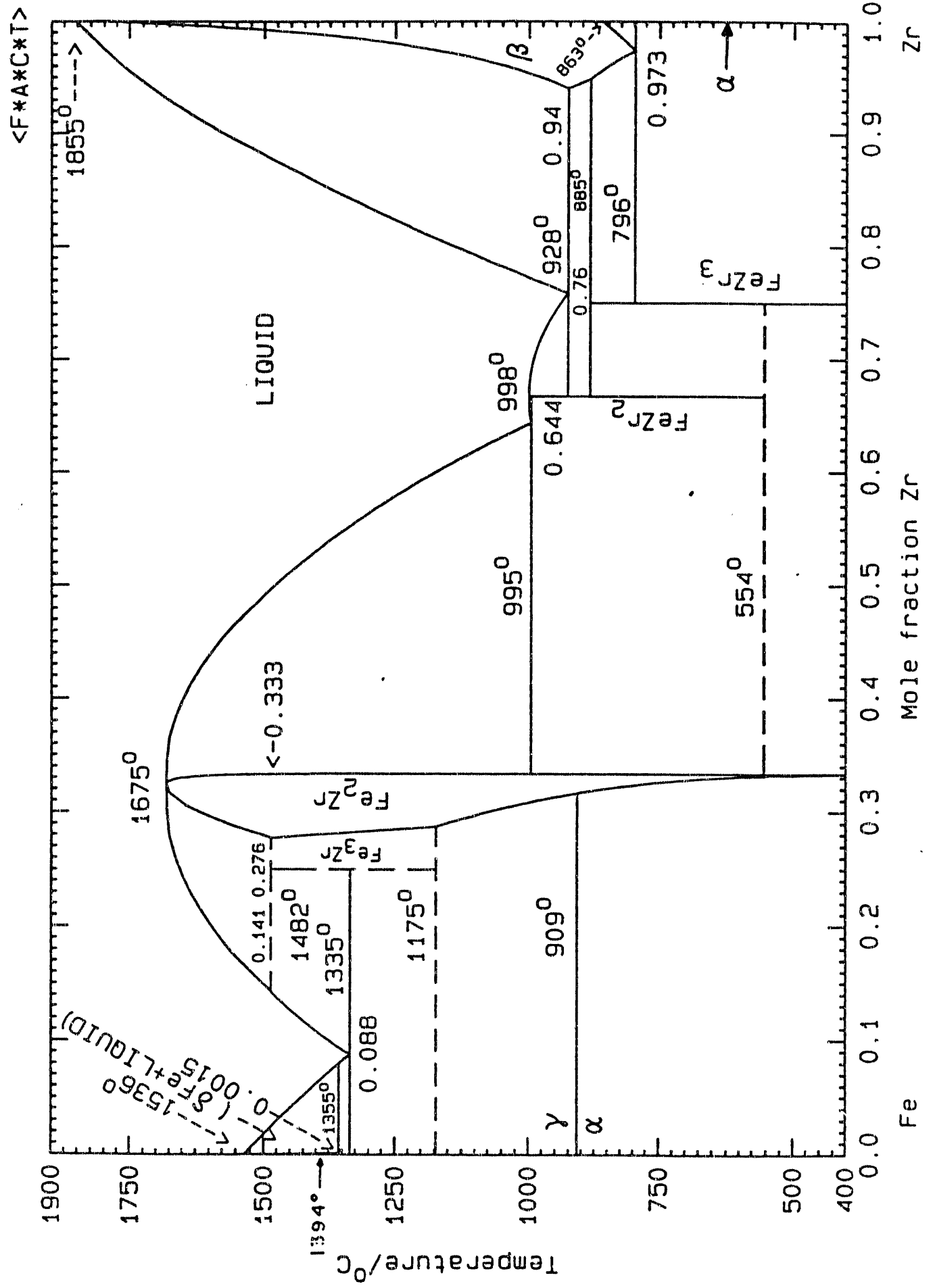

Fig. 3: Optimized Fe-Zr phase diagram.

END

DATE FILMED

9/23/92